Continuum Random Walk Simulations of Diffusion and Reaction in Catalyst Particles

H. P. G. Drewry and N. A. Seaton
Dept. of Chemical Engineering, University of Cambridge, Cambridge CB2 3RA, United Kingdom

To predict the effect of pore structure on the performance of heterogeneous catalysts, a realistic model of the catalyst particle is required. Lattice-based models in which the diffusion and reaction phenomena are restricted to sites and bonds within a regular or irregular lattice are widely used. However, for the realistic simulation of diffusion and reaction in amorphous catalyst supports, such as alumina or silica, a continuum model, which does not artificially restrict the domain in which the reactants are allowed to diffuse, is required.

An efficient method based on a "first passage time" approach is developed for the simulation of diffusion and reaction in a supported catalyst. The model catalyst is composed of spheres representing the support and active sites. By varying the algorithm used to generate the model catalyst, a range of structures can be created. The effect of the structure, and the size and distribution of active sites on the reaction rate is studied.

Introduction

The simulation of diffusion and reaction in a model catalyst particle can help to identify an optimal pore structure for the real catalyst of interest. In order to be effective, the simulations must be carried out using a sufficiently realistic structural model. Lattice-based models, in which diffusion and reaction are restricted to a set of pores of constant cross-section distributed along the bonds of the lattice have been widely used. They are particularly suitable for the simulation of diffusion and reaction in crystalline solids, such as zeolites, but have also been widely used to represent noncrystalline solids such as aluminas and silicas. Sahimi et al. (1990) and Reyes and Iglesia (1993) have reviewed the applications of lattice models, as well as other aspects of modeling diffusion and reaction in porous solids. Recent applications of lattice models include the articles by Beyne and Froment (1990), Arbabi and Sahimi (1991a,b), Sahimi (1992), Zhang and Seaton (1992), McGreavy et al. (1992), Hollewand and Gladden (1992), and Zhdanov (1993). Lattice models are extremely tractable; a number of approximate solutions exist and direct simulation of diffusion and reaction is within the reach of current computers. Another advantage is that many methods for the characterization of porous solids, particularly those based on capillary phenomena such as some adsorption experiments and mercury porosimetry, are based on lattice models (or in some cases on nonintersecting pores of constant cross section). Thus, it is relatively straightforward to relate at least some of the parameters of lattice models to measurements made on real solids. Despite the success of lattice-based models, they suffer from the fundamental limitation that diffusion and reaction in a real amorphous catalyst is not limited to a lattice. It is therefore of interest to consider more realistic simulation methods in which this restriction is relaxed so that diffusion and reaction occur in a continuum. In this article we consider the simulation of bulk (or "molecular") diffusion and heterogeneous reaction in a continuum.

One approach is to simulate diffusion by a random walk through a medium composed of solid elements distributed randomly (but according to some rule) within a continuum. The most straightforward variant of this approach is to give each reactant a sequence of random displacements, the length of each equivalent to the mean free path. If Knudsen diffusion is being simulated, the mean free path of the reactants is much larger than the mean pore size, and the reactant undergoes a series of collisions with the solid phase. In bulk diffusion, the mean free path is much smaller than the mean pore radius. In a simulation of bulk diffusion, which is of interest here, it is possible to use a substitute mean free path that is larger than the real mean free path, but still small

Correspondence concerning this article should be addressed to N. A. Seaton.

compared to the mean pore radius. Even with the substitute mean free path set to the largest acceptable value, the simulation requires a prohibitively large amount of computer time. This observation motivated Zheng and Chiew (1989) to develop a more efficient method. They computed the steady-state rate of a first-order reaction between diffusing fluid-phase reactants and an array of either freely overlapping or nonoverlapping spherical reactive sites distributed randomly within the fluid phase. With their method, the reactants are allowed to advance through the fluid phase in a series of movement steps (see Figure 1a), each one of which represents many individual intermolecular collisions. Each movement step involves the following three substeps: (1) the construction around the reactant of the largest possible "movement sphere" that does not overlap any of the active sites; (2) the selection of the new position for the reactant by choosing a point randomly on the surface of the movement sphere; (3) the calculation of the first passage time (FPT) for the reactant starting at the center of the movement sphere to reach its new location on the surface. The reactant molecule moves through the fluid phase until it gets within a distance δ from the surface of a reactive site when it is considered to have reacted. (With this algorithm, the reactant never actually reaches the surface; Zheng and Chiew (1989) found that accurate results were obtained for $\delta/R_a = 10^{-4}$, where R_a is the radius of the active site.)

In the method of Zheng and Chiew (which for convenience we refer to henceforth as ZC), the time required for the reactant to move from its old position to the new position in each movement step is obtained from the solution of the diffusion equation

$$\frac{\partial P}{\partial t} = D\nabla^2 P \tag{1}$$

where $P(t, x; R)$ is the probability that a reactant starting at point x inside a movement sphere of radius R diffuses and hits the surface of the movement sphere for the first time within the FPT, t; and D is the bulk diffusion coefficient. Equation 1 has a well-known analytical solution in terms of a Fourier series. Zheng and Chiew (1989) computed the FPT for each movement step by sampling from $P(t,x;R)$. This procedure was improved by Torquato and Kim (1989) and, independently, by Zheng and Chiew (1990), who pointed out that only the mean FPT is required, and this is given by Einstein's relation (written here for step i).

$$\tau_{ZC,i} = \frac{R_i^2}{6D} \tag{2}$$

where the subscript ZC is used here to distinguish between this and subsequent FPT results. ZC is most directly applicable to the simulation of diffusion and reaction in homogeneous systems where one reactant is much larger (and therefore more slowly moving) than the other. However, this method cannot be applied directly to simulating diffusion and reaction in a supported catalyst, composed of both active sites and an inert support, for the following reason. The distance that the reactant moves in a single step is equal to the radius of the movement sphere. As the reactant nears the surface of the inert support, the largest possible movement sphere that can be constructed at each step becomes smaller and smaller (see Figure 1b), and so the maximum possible distance that the reactant can move in a single movement step decreases. The reactant therefore spends most of the computer time diffusing near the surface of the inert support, although, of course, in terms of physical time it explores the void phase uniformly. For the system of active sites with no inert support studied by Zheng and Chiew, this problem does not arise as

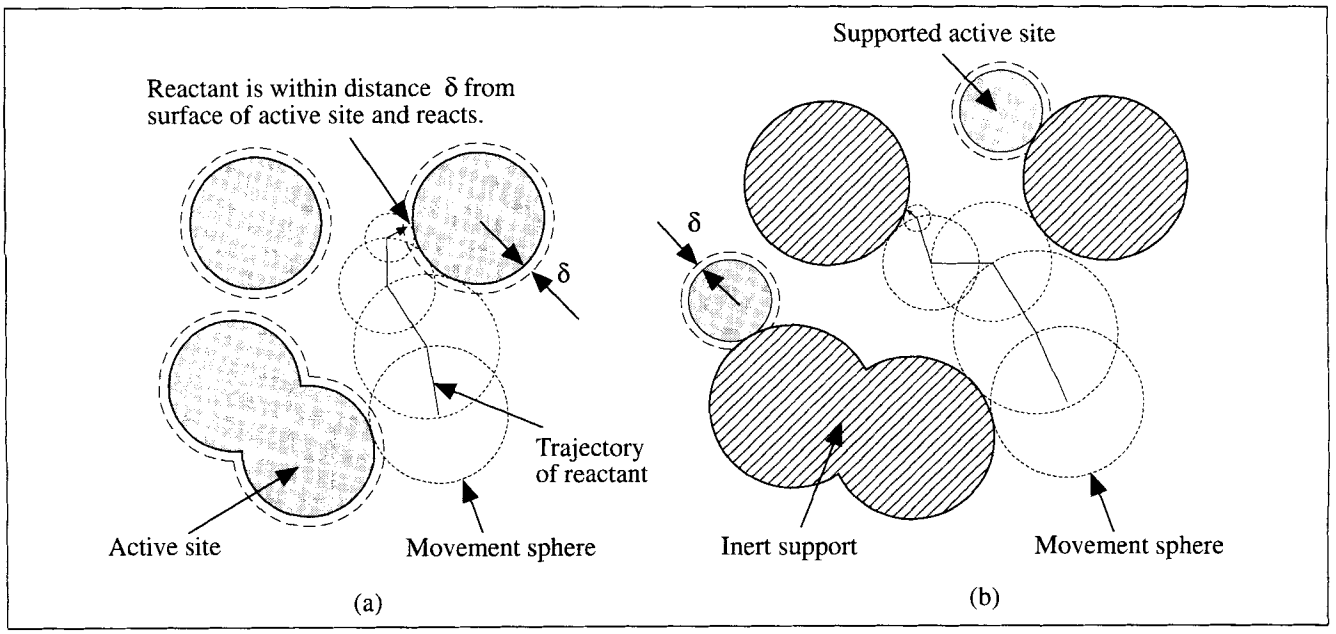

Figure 1. Method developed by Zheng and Chiew (1989).

(a) As applied to a system of static unsupported active sites. (b) As applied to a system of supported active sites. Note that as the reactant moves nearer the surface of the inert support, the sizes of the successive movement spheres become smaller and smaller.

the reactant is removed from the system when it gets within distance δ of the surface.

One way of solving the problem of the reactant spending much of the computer simulation time diffusing near the surface of the inert support would be to use the method developed by Kim and Torquato (1990, 1991, 1992) to compute the effective diffusivity for a range of nonreactive heterogeneous media. With their method, ZC is used to simulate bulk diffusion in all regions except for the intermediate vicinity of an inert surface. For the problem of a molecule diffusing very close to a surface, Kim and Torquato first obtained a series solution for the case of a flat surface. The solution was considerably simplified by restricting the motion of the reactant to movement steps in the direction of the normal of the interface. The solution was adapted, using an approximation, for a curved surface. The error introduced by the previously mentioned restriction and approximation would depend on the size of the movement steps and the geometry of the surface.

Another possible way of solving this problem is to use the hybrid method introduced by Reyes and Iglesia (1991) in their investigation of Knudsen and transitional diffusion in catalyst particles, and subsequently used by Melkote and Jensen (1992), Tassopoulos and Rosner (1992), and Tomadakis and Sotirchos (1993). The hybrid method makes use of ZC plus the discrete random walk method. The discrete random walk method is used whenever the reactant is within a certain distance from the surface of the inert support. Reyes and Iglesia make the point that the radius of the movement sphere must exceed about 5λ, where λ is the mean free path of the reactants so that the number of discrete steps is sufficient for the valid application of the continuum diffusion equation. For bulk diffusion, this restriction does not apply because the length of each random displacement is much less than the smallest characteristic length of the medium.

In both the method of Kim and Torquato (1990, 1991, 1992) and that of Reyes and Iglesia (1991), the molecule advances by FPT steps until it gets close to an inert surface, at which point a different method is used until it is again far from the surface. In this article, we describe a different approach to simulating bulk diffusion and reaction in a supported catalyst, in which FPT calculations are used throughout the simulations (except in certain special cases that occur relatively infrequently). This is accomplished by solving a more general FPT problem (obtaining a solution to Eq. 1 with more general boundary conditions).

The rest of the article is organized in sections as follows. First, we outline the new approach to the simulation of diffusion and reaction in supported catalysts. Second, we give details of the algorithm used to simulate diffusion and reaction in model supported catalysts and show how the new approach can be used to make qualitative inferences about the effect of the morphology on the reaction rate. Finally, in the last section, this article is summarized and the potential of this new approach for making quantitative inferences on the effect of the morphology is discussed.

Simulation Method

The model supported catalyst consists of an inert support formed by an array of spheres, created using some appropriate algorithm (the nature of which determines the final structure), with spherical catalytic sites deposited at random on the surface of the support. The steps in the algorithm of the new method are similar to those in ZC, but instead of constructing around the reactant the largest possible movement sphere that does not overlap any of the active sites or inert support particles (Figure 1b), the movement sphere is constructed so that it just touches the second nearest surface and as a consequence overlaps the particle that forms the nearest surface (Figure 2). With the new method, the constructed movement sphere is always larger than that constructed using ZC, and so the maximum distance that the reactant may move in a single simulation step has been increased. The main advantage of this new method, however, is that the problem of the movement spheres decreasing in size as the reactant diffuses toward the surface of an inert support is solved.

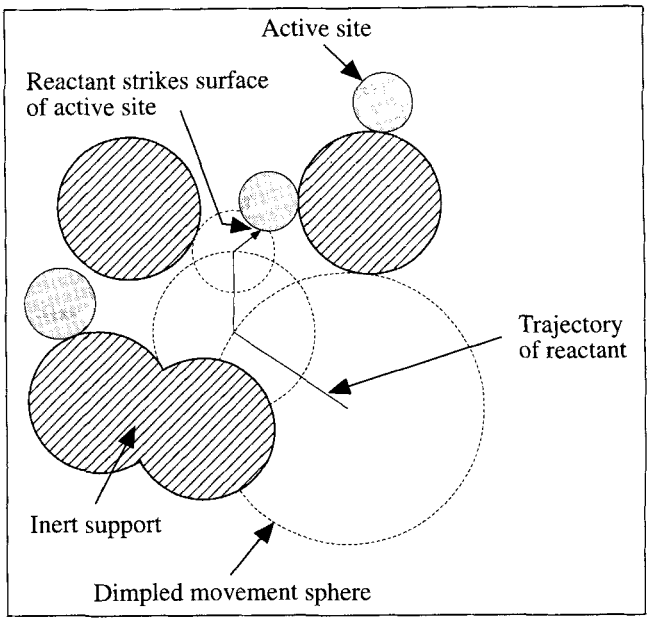

Figure 2. New method applied to a system of supported active sites.

In ZC, the reactant hits all points on the surface of the movement sphere with equal probability and with the same mean FPT. For the "dimpled" movement sphere the probability of hitting a point on the surface, and the corresponding mean FPT, vary with location in a way that depends on the geometry of the dimpled sphere and on whether the dimple is inert (formed by part of the support) or reactive (formed by an active site). In the remainder of this section, we first use a variant of ZC to obtain the hitting point probability density function and the FPT as a function of location on the sphere surface. (This is effectively a numerical solution to Eq. 1 within the dimpled movement sphere.) We then go on to apply these solutions to the simulation of diffusion and reaction in supported catalysts.

Diffusion in dimpled movement spheres

The geometry of a movement sphere for a molecule starting at point p and with a dimple formed by a solid particle centered at point q (Figure 3) is defined by two parameters:

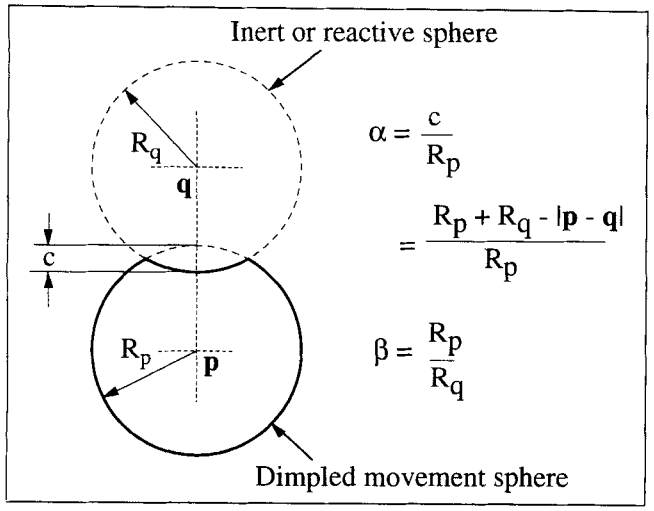

Figure 3. Geometry of the dimpled movement sphere characterized by two parameters.

α gives the degree of eccentricity of the two spheres that constitute the dimpled movement sphere; β gives the size of the dimpled movement sphere relative to that of the sphere that forms the dimple. The surface of the dimpled movement sphere is represented by the bold line. For this dimpled movement sphere, $\alpha = 0.25$ and $\beta = 1$.

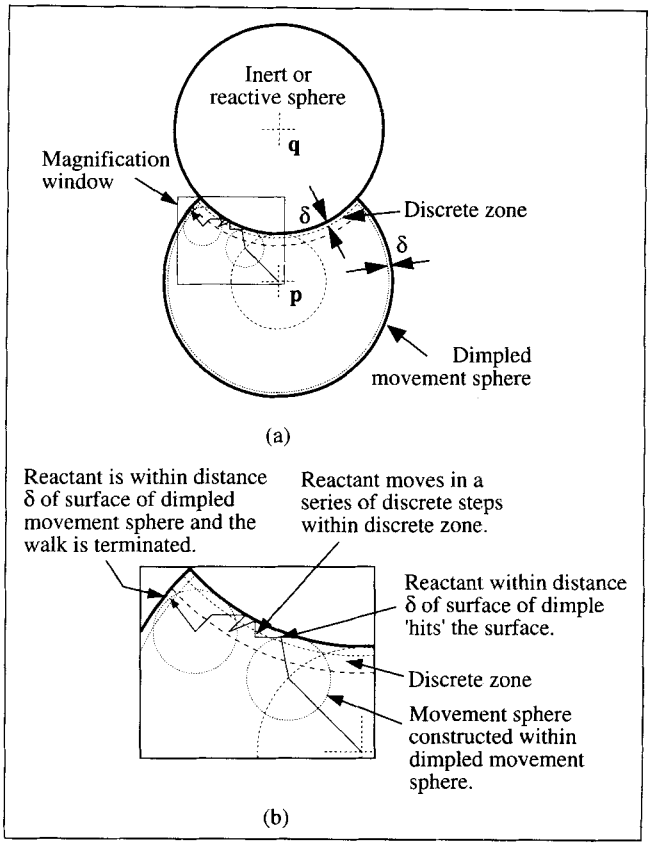

Figure 4. Algorithm of the numerical method used to obtain the distribution of hitting points and corresponding mean hitting times for a dimpled movement sphere.

(b) shows the details of the algorithm inside the magnification window in (a).

$\alpha(=(R_p + R_q - |p - q|)/R_p)$, where R_p is the radius of the movement sphere and R_q is the radius of the dimple, gives the degree of eccentricity of the two spheres; β gives the size of the dimpled movement sphere relative to that of the dimple. The maximum value of α for any dimpled movement sphere is unity, which corresponds to the reactant making contact with the surface of the dimple. The minimum value of α is zero, in which case the dimple is reduced to a point on the surface of the movement sphere.

The simulation of diffusion within the dimpled movement sphere involves placing a reactant molecule at the center of the movement sphere and making it diffuse using ZC until it reaches the nondimpled surface or, if the dimple is reactive, the dimple (Figure 4). (Note that the FPT for a reactant to hit an inert dimple is not of interest.) This procedure is repeated many times until good statistics are obtained for the probability density function for hitting points and the FPT function. For the dimpled movement sphere formed by spheres centered at p and q (Figure 5), the distribution of hitting points and the FPT function is symmetric about the axis pq. The hitting points can be conveniently recorded by dividing the surface of the dimple and the nondimpled surface of the movement sphere into bands as shown in Figure 5. The bands on the surface of the dimple and on the nondimpled surface are delimited by values of θ_q and θ_p, respectively. Once a reactant has hit the surface of the dimple or the nondimpled surface of the movement sphere, a check is made to see what band has been hit and the counter recording the number of times that the band has been hit is incremented. The corresponding elasped time is also noted. In practice, the hitting point probability density function and the FPT can be obtained at the same time for both active and inert dimples, as follows. The first time the reactant hits the dimple (if it does), this contact contributes toward the statistics for the active dimple. The subsequent arrival of this reactant at the nondimpled surface counts only toward the statistics for a movement sphere with an inert dimple. It the reactant does not hit the surface of the dimple before hitting the nondimpled surface, it is counted toward the statistics for movement spheres with both inert and active dimples.

As in the original method of Zheng and Chiew (1989), a parameter δ is defined within which a reactant is considered to have reached the nondimpled surface, or in the case of an active dimple, the surface of the dimple. Parameter δ is set to $10^{-4}\ \zeta$, where ζ is the smaller of R_p and R_q. In order to avoid the problem of drawing increasingly small ZC movement spheres as the reactant nears the surface of the dimple, we switch to a discrete random walk within a certain distance of the dimple surface along the lines of the hybrid method of Reyes and Iglesia (1991). We varied the distance at which the switch between the two methods is made and found the optimal distance to be $10^{-2}\ \zeta$ (the results, as expected, were unaffected). The switch to the discrete random walk is necessary so that after the reactant has hit the surface of the dimple, it is able to continue diffusing until it hits the nondimpled surface.

One step using ZC inside the dimpled movement sphere

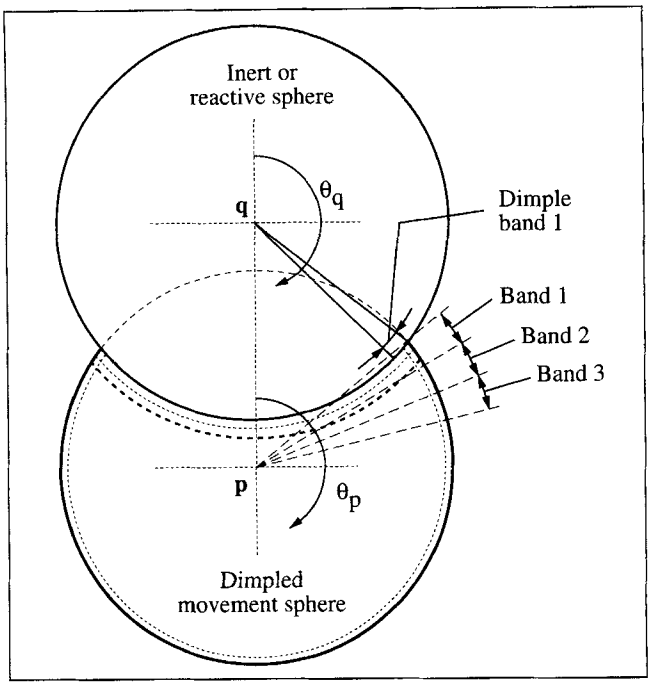

Figure 5. Surface of the dimpled movement sphere is divided into two parts: the surface of the dimple and the nondimpled surface of the dimpled movement sphere.

Each part is divided into latitudinal bands that are used to record the distribution of hitting points. For this dimpled movement sphere, $\alpha = 0.75$ and $\beta = 1$.

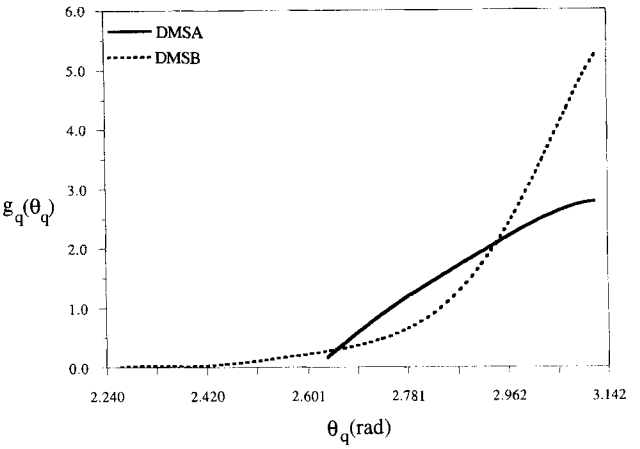

Figure 6. Probability density function for hitting a point on the surface of the dimple, $g_q(\theta_q)$, as a function of location on the surface defined by θ_q for two different dimpled movement spheres.

DMSA ($\alpha = 0.25$, $\beta = 1$) and DMSB ($\alpha = 0.75$, $\beta = 1$).

involves the following substeps: (1) a movement sphere centered on the reactant is constructed so that it just touches either the surface of the dimple or the nondimpled surface of the dimpled movement sphere, whichever is the nearer; (2) a position on the surface of the movement sphere with radius R is chosen at random; (3) the mean FPT required for the reactant to move to its new position on the surface of the movement sphere from its old position is computed. It is convenient to rewrite Eq. 2 in dimensionless form as

$$\tau^*_{ZC,i} = \frac{\tau_{ZC,i} D}{R_p^2} = \frac{1}{6}\left(\frac{R}{R_p}\right)^2 \tag{3}$$

where the subscript ZC is used to indicate a step using ZC within the dimpled movement sphere. The superscript * is used here and elsewhere to indicate that the variable is dimensionless.

One step using the discrete random walk method inside the dimpled movement sphere involves giving the reactant a random displacement of size $l = 10^{-2}\,\zeta$. If the new position for the reactant is outside the boundary of the dimpled movement sphere, l is reduced so that the new position is at the boundary. The dimensionless time for step j is given by

$$t^*_{d,j} = \frac{1}{3}\left(\frac{l}{R_p}\right)^2. \tag{4}$$

The subscript d indicates that the simulation step involves the discrete random walk method. Equation 4 is the standard equation describing a discrete random walk (Reyes and Iglesia, 1991).

The dimensionless mean FPT, τ^*, is the sum of the times for all ZC steps given by Eq. 3 and the discrete steps given by Eq. 4:

$$\tau^* = \sum_i \tau^*_{ZC,i} + \sum_j t^*_{d,j}. \tag{5}$$

Distributions were obtained for eight values of both α and β. The values of α used were: 0.05, 0.25, 0.5, 2/3, 0.75, 0.84, 0.92, 1.0. The values of β were: 3, 2, 1, 0.5, 0.3, 0.1, 0.07, 0.01. Note that (from the geometry of the movement sphere) for $\beta = 3$, α is restricted to be less than 2/3. In order to generate accurate statistics, the diffusion of 1.5×10^6 reactants was simulated for each movement sphere geometry. As an example of the type of results obtained, Figures 6–9 show the distributions of hitting points and the corresponding mean FPT obtained for two different dimpled movement spheres: the dimpled movement sphere shown in Figure 3 ($\alpha = 0.25$, $\beta = 1$), henceforth referred to as DMSA, and the dimpled movement sphere shown in Figure 5 ($\alpha = 0.75$, $\beta = 1$), henceforth referred to as DMSB. The distributions obtained for the case of the reactive dimple and also that of the inert dimple are shown.

With DMSA, the value of θ_q (see Figure 5) that defines the intersection line between the dimple surface and the nondimpled surface is 2.636 rad. The corresponding value for θ_p is 0.505 rad, so the entire surface of the dimpled movement sphere is defined by ($2.636 \le \theta_q \le \pi$) and ($0.505 \le \theta_p \le \pi$). For DMSB, the entire surface of the dimpled movement sphere is defined by ($2.246 \le \theta_q \le \pi$) and ($0.896 \le \theta_p \le \pi$). The probability that the surface of the dimple is hit is 0.103 for DMSA and 0.547 for DMSB.

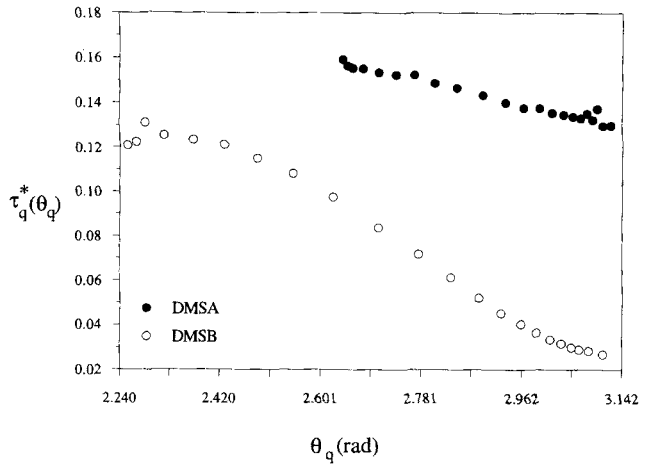

Figure 7. Mean FPT for the surface of dimple, $\tau_q^*(\theta_q)$, as a function of location on the surface defined by θ_q for two different dimpled movement spheres.

DMSA ($\alpha = 0.25$, $\beta = 1$) and DMSB ($\alpha = 0.75$, $\beta = 1$).

Figures 6 and 7 show, respectively, the probability density function for hitting a point on the surface of the dimple and the corresponding mean FPT, $\tau_q^*(\theta_q)$, as a function of location on the surface for both DMSA and DMSB. The probability density function, g_q, as a function of the polar angle, θ_q, is normalized by:

$$\int_0^{\pi} g_q(\theta_q) 2\pi R_q \sin(\theta_q)\, d\theta_q = 1. \tag{6}$$

It can be seen in Figure 6 that for both DMSA and DMSB, $g_q(\theta_q)$ is highest for the position on the surface of the dimple that is closest to the starting point of the reactant ($\theta_q = \pi$), decreasing continuously with decreasing θ_q. This is expected, since the surface of the dimple and the nondimpled surface will become closer to each other as θ_q decreases and "compete" for the reactant. The reason for the difference in the shape of the plots can be explained: a reactant that is diffusing toward the region close to the intersection line will on entering this region be close to both the surface of the dimple and the nondimpled surface. The reactant will tend to hit either surface and be removed before it has had a chance to diffuse further toward the intersection line. The resulting effect is the lowering of the probability of the reactant hitting a surface close to the intersection line. The strength of this effect, which depends on the curvature of the dimple, is greater in DMSB than in DMSA.

It can be seen from the plots in Figure 7 that $\tau_q^*(\theta_q)$ is, as expected, greater in DMSA than in DMSB, reflecting the larger distance on average that the reactant has to diffuse before hitting the dimple surface.

Figures 8 and 9 show, respectively, the probability density function for hitting a point on the nondimpled surface and the corresponding FPT, $\tau_p^*(\theta_p)$, as a function of location on the surface for both reactive and inert dimples. The probability density function, g_p, as a function of the polar angle, θ_p, is normalized by

$$\int_0^{\pi} g_p(\theta_p) 2\pi R_p \sin(\theta_p)\, d\theta_p = 1. \tag{7}$$

The plots in Figure 8 for both DMSA and DMSB with a reactive dimple surface show how $g_p(\theta_p)$ for the same reasons behaves in a similar way to $g_q(\theta_q)$.

For the case of the inert dimple, there are two opposing effects that influence the plots of $g_p(\theta_p)$. One of the effects, which reduces the probability of the reactant hitting the nondimpled surface close to the intersection line (similar to that described earlier for the dimple surface), is caused by the reactant diffusing toward the intersection line being

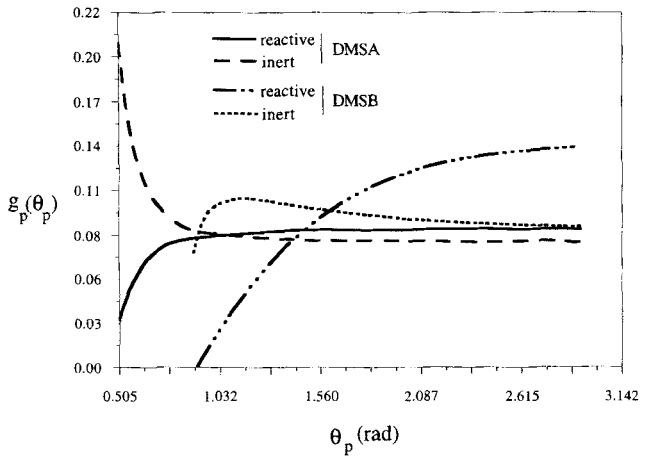

Figure 8. Probability density function for nondimpled surface $g_p(\theta_p)$, as a function of location on the nondimpled surface defined by θ_p for two different dimpled movement spheres (with reactive or inert dimple).

DMSA ($\alpha = 0.25$, $\beta = 1$) and DMSB ($\alpha = 0.75$, $\beta = 1$).

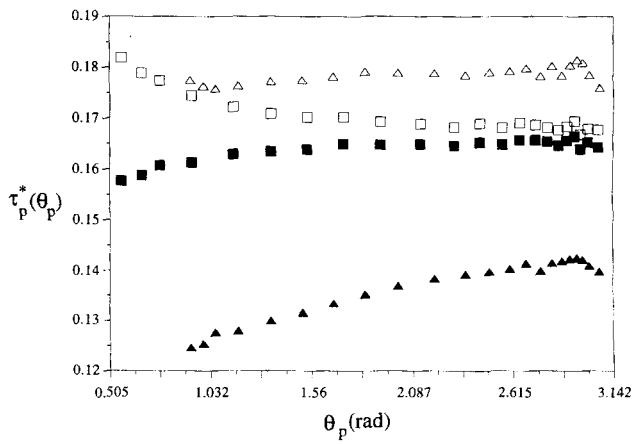

Figure 9. Mean FPT for nondimpled surface, $\tau_p^*(\theta_p)$, as a function of location on the nondimpled surface defined by θ_p for two different dimpled movement spheres (with reactive or inert dimple).

DMSA ($\alpha = 0.25$, $\beta = 1$) and DMSB ($\alpha = 0.75$, $\beta = 1$). The legend used is as follows: DMSA with reactive dimple (■), DMSA with inert dimple (□), DMSB with reactive dimple (▲), DMSB with inert dimple (△).

forced to diffuse in a narrow region close to the inert dimple surface and the nondimpled surface. The reactant will tend to hit the nondimpled surface and be removed before it has had a chance to diffuse further toward the intersection line. The second effect is due to the reflective nature of the dimple surface; the reactant, on hitting the dimple, will continue to diffuse until it hits the nondimpled surface. The effect of the inert dimple is to "channel" the reactants toward the intersection line, thus increasing the probability of the reactant hitting the nondimpled surface close to the intersection line. The relative strength of the two opposing effects will depend on the curvature of the dimple. In DMSA close to the intersection line, the channel effect dominates, and thus $g_p(\theta_p)$ increases with decreasing θ_p.

From Figure 9, it can be observed that for any value θ_p, the value of the mean FPT is greater for the case of an inert dimple than that of a reactive dimple, reflecting the fact that in the latter case some of the reactants that hit the nondimpled surface have reflected from the dimple.

Application of the dimpled sphere solutions

Having solved the problem of diffusion and reaction in dimpled movement spheres of a range of geometries, diffusion and reaction in a model-supported catalyst can now be simulated by moving the reactant by a sequence of dimpled sphere (DS) steps until it reacts on one of the active sites. In each DS step involving an inert dimple, a hitting point is selected at random from the appropriate distribution function, $g_p(\theta_p)$, and the corresponding FPT calculated from $\tau_p^*(\theta_p)$. The functions $g_p(\theta_p)$ and $\tau_p^*(\theta_p)$ are obtained for the required values of α and β by interpolating quadratically in these two variables among the simulation results for the dimpled movement sphere. In the case of a DS step involving a reactive dimple, the probability that the reactant hits the dimple is obtained from the dimpled sphere solution, the hitting point is selected at random from $g_p(\theta_p)$ or $g_q(\theta_q)$ as appropriate and the corresponding FPT calculated from $\tau_p^*(\theta_p)$ or $\tau_q^*(\theta_q)$, again interpolating as required between the dimpled-sphere simulation results.

The mean FPT for step k, τ_k, is calculated by rescaling the dimensionless value obtained by interpolating the dimpled movement sphere results, τ_k^*:

$$\tau_{DS,k} = \frac{\tau_k^* R_k^2}{D}, \tag{8}$$

where R_k is the radius of the movement sphere at step k. The subscript DS indicates that the simulation step involves the construction of a dimpled movement sphere.

Because of the function evaluations and interpolation involved, each DS step is computationally more expensive than a ZC step. In most cases, this is compensated for by the increased distance that the reactant can move in a single simulation step. However, if the particle that forms the dimple barely penetrates the movement sphere, it is more efficient to slightly reduce the radius of the movement sphere, so that the dimple disappears, and use a ZC step instead. Our experience indicates that the value for α below which it is more efficient to reduce the radius of the movement sphere in this way is 0.2. (This figure will presumably depend weakly on the algorithm and computer hardware used.)

Another computational simplification can be made if the movement sphere is much smaller than the dimple. In this case, the reactant at the center of the dimpled movement sphere perceives the surface of the dimple as flat. We have found that the value for β below which the surface of the dimple may be regarded as flat is approximately 0.01. If the value of β falls below this, then the distribution of hitting points and corresponding mean hitting times obtained for $\beta = 0.01$ can be used with the FPT appropriately rescaled.

An additional type of simulation step is required if the support particles are allowed to overlap during the generation of the model catalyst. Because the radii of successive dimpled movement spheres decrease as the reactant diffuses toward an intersection line formed by two overlapping support particles, the maximum distance that the reactant can move in a simulation step decreases to very small values until the molecule spends almost all the computer time diffusing close to the intersection line. This is analogous to the problem arising with ZC, except that by using our new method the reactant is "attracted" to a one-dimensional object rather than a two-dimensional one. This problem is avoided by using a discrete random walk, with initial step length, $l = 0.01 R_s$ where R_s is the radius of the support particles, to dislodge the reactant. (As in the simulation of diffusion within the dimpled movement sphere, the step length is reduced if a step of the original length enters the solid phase.) The time for discrete step m is given by

$$t_{d,m} = \frac{l^2}{3D}. \tag{9}$$

The survival time, t_S, of the reactant is the sum of the times for dimpled movement sphere steps, given by Eq. 8, the times for the ZC steps, given by Eq. 2, and the times for the discrete steps, given by Eq. 9:

$$t_S = \sum_i \tau_{ZC,i} + \sum_k \tau_{DS,k} + \sum_m t_{d,m}. \tag{10}$$

Random walks are carried out for many reactants in each realization of the model catalyst, formed using a sufficient number of configurations, in order to obtain results representative of a macroscopic catalyst particle. The first-order rate constant, k, is given by

$$k = \frac{1}{\langle t_S \rangle} \tag{11}$$

where $\langle\ \rangle$ indicates an average over all reactants and configurations constituting the realization of the model catalyst.

Results

Unsupported active sites

In order to check the accuracy and also the efficiency of the new method, the simulations reported by Zheng and Chiew (1989, 1990) were repeated using both ZC and the new method (Figures 10 and 11). Systems of spherical particles, representing the active sites, were created using the method

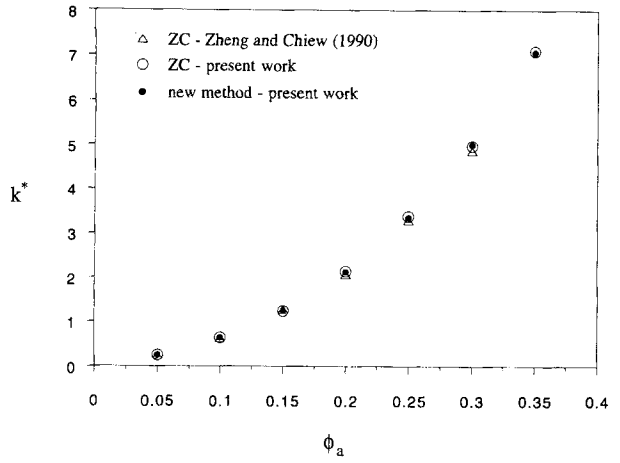

Figure 10. Dimensionless reaction rate, k^*, as a function of active site volume fraction, ϕ_a, for 50 nonoverlapping spherical active sites using ZC and the new method.

The results reported by Zheng and Chiew (1990) using ZC are also shown.

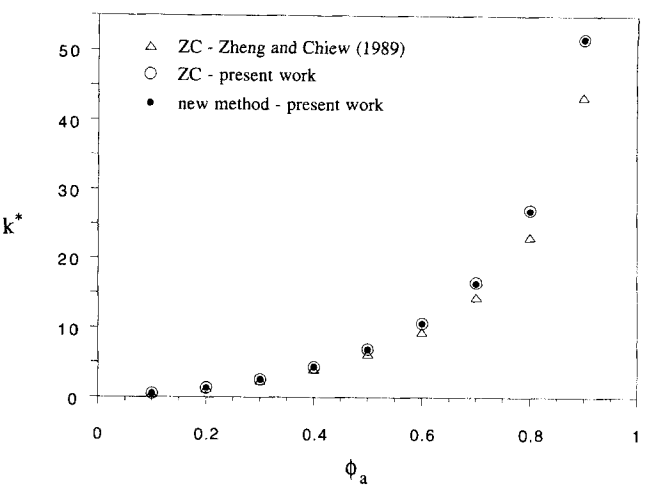

Figure 11. Dimensionless reaction rate, k^*, obtained as a function of active site volume fraction, ϕ_a, for 100 overlapping spherical active sites using ZC and the new method.

The results reported by Zheng and Chiew (1989) using ZC are also shown. Note that in the simulations carried out by Zheng and Chiew, the time for each simulation step was obtained from a distribution and not Eq. 2.

of random sequential addition (RSA). For a system of overlapping active sites, the particles that represent the active sites are added to randomly chosen locations within a cubical cell until the desired number density of particles is achieved. For nonoverlapping active sites, the method is unchanged except that it is necessary to check whether the particle that is added overlaps any of the particles already added. If there is overlap, the particle is rejected and another is added. Periodic boundary conditions were used in order to minimize the finite-size effect. The parameters of Zheng and Chiew (1989) were used as follows. Each configuration consisted of 50 spherical particles in the case of nonoverlapping active sites and 100 in that of overlapping sites. The results were obtained by averaging over ten configurations and 10^5 diffusing reactants.

In Figures 10 and 11, simulated values of the dimensionless reaction rate, k^*, given by

$$k^* = \frac{kR_a^2}{D} \tag{12}$$

are displayed as a function of the volume fraction of unsupported active sites, ϕ_a. For a system of nonoverlapping particles with radius R_a and number density ρ the volume fraction of the particles is given by

$$\phi_a = \eta \tag{13}$$

where η $(= \rho 4\pi R_a^3/3)$ is the reduced number density. For particles that are overlapping, the volume fraction is given by

$$\phi_a = 1 - \exp(-\eta). \tag{14}$$

The plots shown in Figures 10 and 11 show that there is a systematic, though very small, difference between the results reported by Zheng and Chiew (1989, 1990) using their method and those obtained by the authors using the same method for both overlapping and nonoverlapping active sites. It is clear, however, that the results obtained by the authors using both the ZC and the new method agree very well. The calculated deviates show that the two sets of data obtained using ZC and the new method for both overlapping and nonoverlapping active sites are not significantly different at the 95% level; the good agreement between the two sets of data underlies the accuracy of the new method.

When applied to systems of unsupported active sites, the new method is approximately 3 times faster than ZC. We emphasize that our main motivation for the development of the new method is that ZC cannot be applied to a supported catalyst. The increase in efficiency in the simulation of systems of unsupported active sites is incidental.

Supported active sites

The first step is to define a set of "construction rules" for the creation of the model catalyst. These rules might be chosen to reproduce what is known of the morphology of the real catalyst of interest, or in order to investigate some particular model structure. The rules are not necessarily directly related to the real catalyst manufacturing process. For each model supported catalyst, the inert support was created using the penetrable concentric shell (PCS) model (Torquato, 1984). In the PCS model, the spherical particles consist of an impenetrable core of radius ϵR_s and a penetrable concentric shell of thickness $(1-\epsilon)R_s$, where ϵ $(0 \le \epsilon \le 1)$ gives the degree of impenetrability of the particles. The lower and upper limits of ϵ correspond to the cases of overlapping and nonoverlapping particles, respectively. By changing ϵ, the connectedness of the inert support particles is changed.

Two different methods were used to create the configurations of the support particles: RSA, and the method of Metropolis et al. (1953), which creates configurations of par-

ticles in thermal equilibrium. In the Metropolis method, particles are repeatedly given small, random displacements. If the hard core of the particles that is moved overlaps the hard core of any other particle, the move is rejected. After each particle move, the configuration of the system has changed only slightly, so a large number of moves is required to generate each configuration of the model support. Following Miller and Torquato (1990), we moved each particle 80 times between configurations. Periodic boundary conditions were used for both equilibrium and RSA configurations.

For a system of spheres created using RSA, the maximum volume fraction of the support particles that can be achieved is limited by the close packing fraction of the hard core (~ 0.41). The corresponding value for η ($= \rho 4\pi R_s^3/3$) is given by

$$\eta \approx 0.41\epsilon^{-3}. \tag{15}$$

For a system of nonoverlapping spheres ($\epsilon = 1$) created using the Metropolis method, the maximum volume fraction of the support particles that can be achieved is higher than that for RSA, ~ 0.63. The corresponding value for η is given by

$$\eta \approx 0.63\epsilon^{-3}. \tag{16}$$

The morphology of the support was varied by changing the volume fraction of the inert support particles, ϕ_s, and the impenetrability parameter, ϵ. For the case of nonoverlapping inert support particles ($\epsilon = 1$) and overlapping inert support particles ($\epsilon = 0$), the volume fraction is computed using Eqs. 13 and 14, respectively. For intermediate values of ϵ, the calculation of the volume fraction is not trivial. For equilibrium systems, the analytical approximation developed by Rikvold and Stell (1985) for the PCS model can be used. The volume fraction of the support is given by

$$\phi_s(\epsilon, \eta) = 1 - u(\epsilon, \eta)w(\epsilon, \eta) \tag{17}$$

where $u(\epsilon, \eta)$ is given by

$$u(\epsilon, \eta) = (1 - \epsilon^3\eta)\exp\left[-\frac{(1-\epsilon^3)\eta}{1-\epsilon^3\eta}\right] \tag{18}$$

and $w(\epsilon, \eta)$ is given by

$$w(\epsilon, \eta) = \exp\left\{-\frac{3\epsilon^3\eta^2}{2(1-\epsilon^3\eta)^3} \times [2 - 3\epsilon + \epsilon^3 - \epsilon^3\eta(3\epsilon - 6\epsilon^2 + 3\epsilon^3)]\right\}. \tag{19}$$

Note that for $\epsilon = 1$ and $\epsilon = 0$, Eqs. 17–19 reduce to Eqs. 13 and 14, respectively. Lee and Torquato (1988) carried out computer simulations to find the porosity as a function of η and ϵ for a number of different equilibrium configurations. They found that the computed porosities compared favorably with the porosities predicted using Eqs. 17–19.

We carried out a check to see if Eqs. 17–19 could also be used for model catalysts using RSA systems. The method used involved using Eqs. 17–19 to compute η for given values of ϕ_s and ϵ, which was then used to set the dimensions of the cubical cell containing the centers of a fixed number of support particles. The volume fraction of the support was then computed by generating a large number of points within the system and computing the fraction of the points that were found to be inside a support particle. Equilibrium as well as RSA systems were created for comparison purposes. The results that were obtained by the averaging over 500 different configurations and 10,000 points each configuration are summarized in Table 1. For each input value of ϕ_s, the computed value of ϕ_s and the associated standard error for both RSA and equilibrium systems for different values of ϵ are included in the table. By comparing the results obtained for RSA and equilibrium systems, it can be seen that the approximation works almost as well for RSA systems as for equilibrium systems. The largest error encountered was for the case where $\epsilon = 0.5$ and $\phi_s = 0.9$. Because the error at most is approximately 1.5%, Eqs. 17–19 were used in this work to set the dimensions of the cubical cell for both RSA and equilibrium systems.

The construction of the model-supported catalyst is completed by adding the required number of spherical active sites to the surface of the support; the sites were added by random sequential addition. The active sites are not permitted to overlap either the inert support particles or any of the other

Table 1. Monte Carlo Simulation Data for the Volume Fraction of Support Particles for Values of the Impenetrability Parameter, ϵ*

ϕ_s		$\epsilon = 0.0$	$\epsilon = 0.25$	$\epsilon = 0.5$	$\epsilon = 0.625$	$\epsilon = 0.75$	$\epsilon = 0.875$	$\epsilon = 1.0$
0.1	EQM	—	0.1002 ± 0.0002	0.1001 ± 0.0001	0.1000 ± 0.0001	0.1001 ± 0.0001	0.1000 ± 0.0001	0.1000 ± 0.0001
	RSA	0.0997 ± 0.0002	0.1001 ± 0.0001	0.1003 ± 0.0001	0.1000 ± 0.0001	0.1001 ± 0.0001	0.1000 ± 0.0001	0.1003 ± 0.0001
0.3	EQM	—	0.3011 ± 0.0004	0.3006 ± 0.0003	0.3002 ± 0.0002	0.2998 ± 0.0002	0.2998 ± 0.0002	0.2998 ± 0.0002
	RSA	0.3001 ± 0.0004	0.2999 ± 0.0004	0.3008 ± 0.0003	0.3007 ± 0.0002	0.3006 ± 0.0002	0.3002 ± 0.0002	0.3001 ± 0.0002
0.5	EQM	—	0.5018 ± 0.0007	0.5012 ± 0.0004	0.4997 ± 0.0003	0.4990 ± 0.0003	0.4992 ± 0.0002	0.5003 ± 0.0002
	RSA	0.5007 ± 0.0008	0.5022 ± 0.0007	0.5028 ± 0.0004	0.5025 ± 0.0003	0.5018 ± 0.0002	0.4992 ± 0.0002	—
0.7	EQM	—	0.7046 ± 0.0009	0.7010 ± 0.0006	0.6992 ± 0.0004	0.6978 ± 0.0003	0.6981 ± 0.0002	—
	RSA	0.702 ± 0.001	0.705 ± 0.001	0.7072 ± 0.0006	0.7065 ± 0.0004	0.7001 ± 0.0003	—	—
0.9	EQM	—	0.9045 ± 0.0009	0.9003 ± 0.0005	0.8971 ± 0.0004	0.8965 ± 0.0002	—	—
	RSA	0.904 ± 0.001	0.905 ± 0.001	0.9130 ± 0.0005	0.9075 ± 0.0003	—	—	—

*For each required input value of ϕ_s, the computed values of ϕ_s for the equilibrium (EQM) and RSA systems are listed. The errors are standard errors.

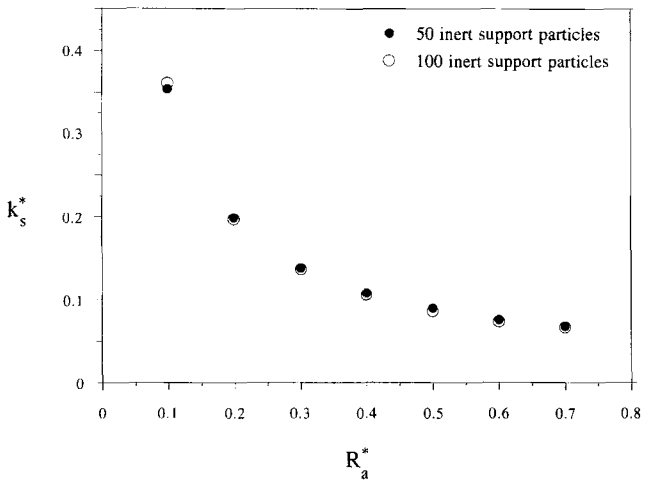

Figure 12. Dimensionless reaction rate, k_s^*, as a function of the dimensionless radius of active sites, R_a^*.

The parameters were set as follows: $\phi_s = 0.35$, $S^* = 0.05$, $\epsilon = 0.5$.

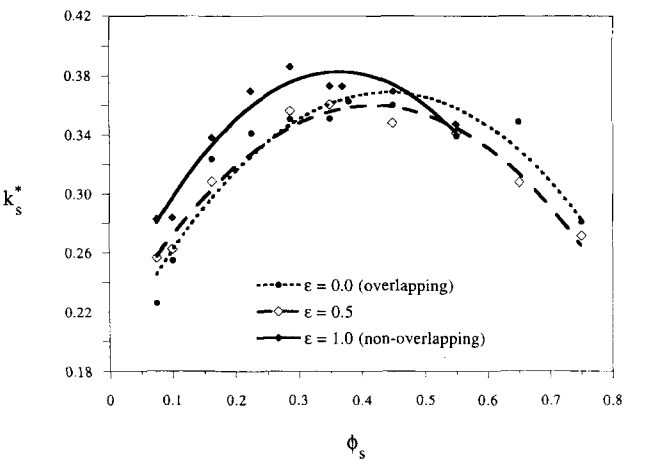

Figure 13. Dimensionless reaction rate, k_s^*, as a function of volume fraction of inert support, ϕ_s, for different values of the impenetrability parameter, ϵ.

The parameters were set as follows: $R_a^* = 0.1$, $S^* = 0.05$. Curves have been drawn to help guide the eye.

active sites already added. Experimentally, this process corresponds to the deposition of active material randomly within the pore volume. The specific surface area, in dimensionless form, is given by $S^* = A_a R_s / V$. Here, $V\ (=(1-\phi_s)L^3)$ is the pore volume, where L is the length of the cubical cell; A_a is the total surface area of the active sites.

Note that the computed number of active sites required to give the desired specific surface area of active sites will not in general be an integer. It is therefore necessary to use a weighted average of two integer values for the number of active sites, one that is above and one that is below the required number of active sites.

The results of a number of different sets of simulations carried out to investigate the effect of the catalyst morphology on the reaction rate are now presented. The results were in general obtained by averaging over 20 different configurations of the solid phase and 5×10^3 reactants unless indicated otherwise.

In all the simulations, a cubical cell containing the centers of approximately 50 spherical particles surrounded by periodic images of itself was used to represent the inert support in the model catalysts. A set of simulations was carried out to check whether finite size effects were significant. The results, which are shown in Figure 12, show the dimensionless reaction rate, k_s^*, given by

$$k_s^* = \frac{kR_s^2}{D} \tag{20}$$

plotted as a function of the dimensionless radius of the active sites, $R_a^*(= Ra/R_s)$. The subscript, s, is used to distinguish this dimensionless reaction rate from that defined in Eq. 12. The inert support created using RSA consisted of either 50 or 100 spherical particles. The standard errors range from 1 to 5 percent, the larger errors corresponding to the larger radii of active sites. The agreement between the two sets of data is very good, suggesting that finite size effects are not significant. The shape of the plots can be explained straightforwardly. As the radius is decreased, the number of required active sites to give a certain specific surface area increases, and so the reactant will on average take less time to diffuse and hit an active site and thus react.

The plots in Figures 13 and 14 show k_s^* plotted as a function of ϕ_s for different values of ϵ. In these figures, the dimensionless specific area of active sites, S^*, is 0.05. In Figure 13, the dimensionless radius, R_a^*, of all the active sites is 0.1, whereas in Figure 14, R_a^* is 0.4. The standard errors are approximately 2%, the largest being 2.7%. The results were obtained by averaging over 20 different configurations and 5×10^4 reactants.

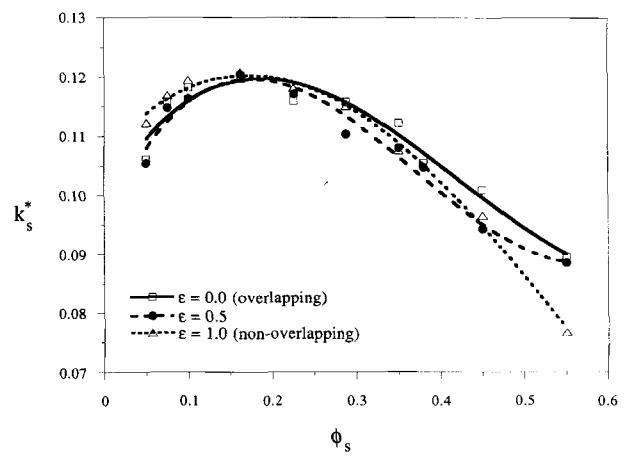

Figure 14. Dimensionless reaction rate, k_s^*, as a function of volume fraction of inert support, ϕ_s, for different values of the impenetrability parameter, ϵ.

The parameters were set as follows: $R_a^* = 0.4$, $S^* = 0.05$. Curves have been drawn to help guide the eye.

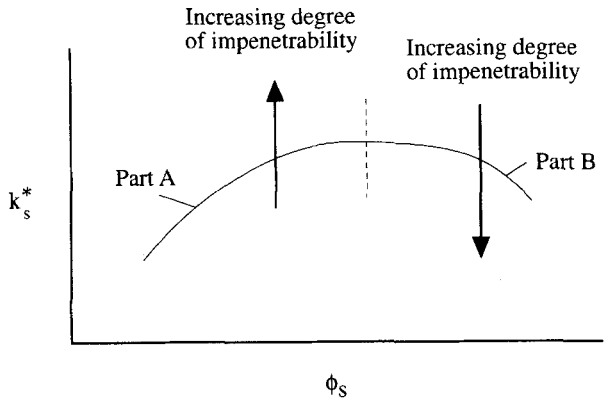

Figure 15. Effect of the degree of impenetrability on the reaction rate as a function of the volume fraction of the inert support.

To help with the interpretation of the plots, Figure 15 has been drawn to show how the plots are affected by the radius of the active site and also the degree of impenetrability. In Part A of Figure 15, the reaction rate increases with increasing volume fraction, as seen in the plot shown in Figure 13 and also in part of the plot shown in Figure 14. As the volume fraction of inert support increases, some of the pores become too narrow to accommodate an active site and so the active sites rather than being evenly dispersed throughout the pore volume (see Figure 16a) start to concentrate in the larger pores (see Figure 16b). As a large proportion of transport takes place in the larger pores, the reactant will on average take less time to hit an active site and react and the reaction rate therefore increases. Increasing the impenetrability of the inert support particles has the effect of increasing the number of smaller sized pores while reducing the number of larger sized pores. The reaction rate therefore increases with increasing degree of impenetrability.

In Part B of Figure 15, the reaction rate decreases with increasing volume fraction of inert support, as seen in the plots shown in Figures 13 and 14. Because the volume fraction of the inert support is high, smaller pores predominate and the active sites therefore concentrate in the pockets (see Figure 16c). With some of the active sites clumped together, the reactant is forced to travel further before hitting an active site than it would if the active sites were dispersed. The clumping together of active sites increases with increasing volume fraction of inert support. Increasing the degree of impenetrability, and thus the proportion of relatively small pores, increases the clumping effect and so the reaction rate decreases with increasing degree of impenetrability. For a given volume fraction of support, the extent of clumping increases with the size of the active sites. Consequently, the maximum reaction rate occurs at lower values of ϕ_s as R_a^* increases, as may be seen by comparing Figures 13 and 14.

In these simulations, equilibrium as well as RSA systems were used to represent the inert support so that model catalysts with higher inert support volume fractions could be created. A similar set of simulations (see Figure 17) was carried out to investigate whether results for model catalysts with inert supports created using either RSA or equilibrium systems

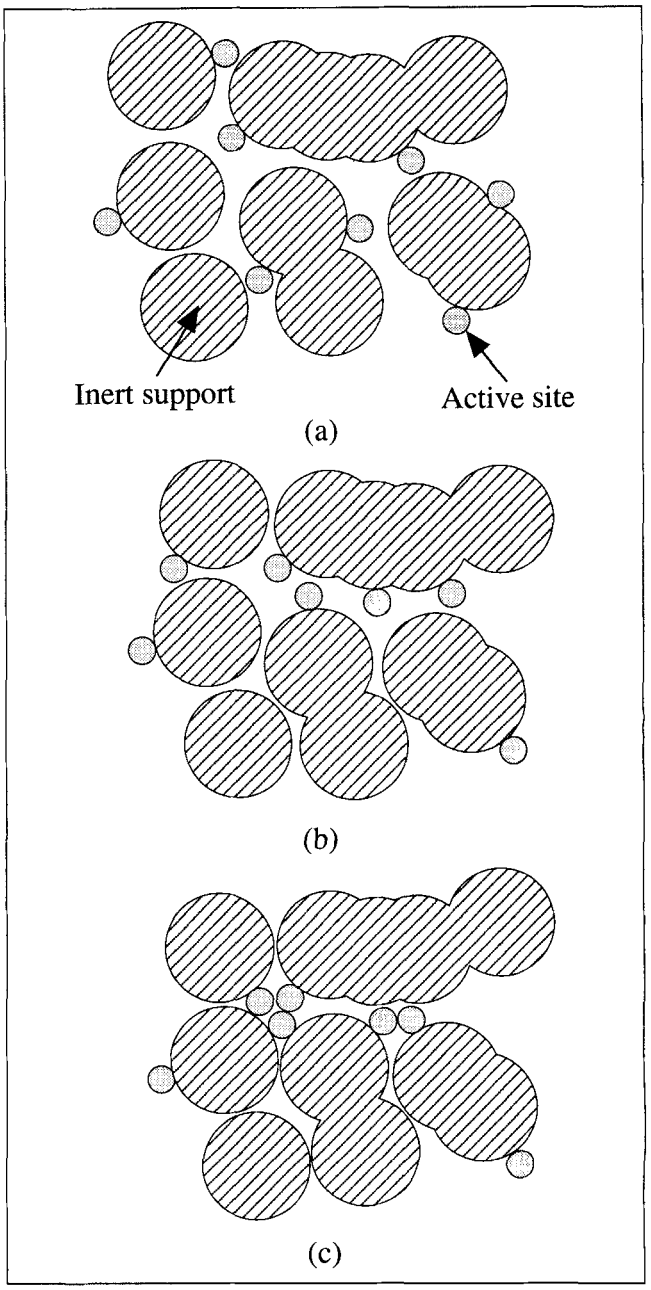

Figure 16. Effect of increasing the volume fraction of inert support.

(a) With a relatively low volume fraction of inert support, the active sites are fairly uniformly dispersed; (b) as the volume fraction of inert support is increased, the active sites concentrate in the larger pores; and (c) as the volume fraction of inert support is increased further, the active sites start to clump together in the pockets.

are different. An analysis of the data showed no significant difference at the 95% confidence level.

A set of simulations was carried out in which the impenetrability parameter, ϵ and the dimensionless radius of the active sites, R_a^*, were kept constant at 0.5 and 0.1, respectively, while the parameters S^* and ϕ_s were varied. Figure 18 shows plots of k_s^* as a function of S^* for different values of ϕ_s. In

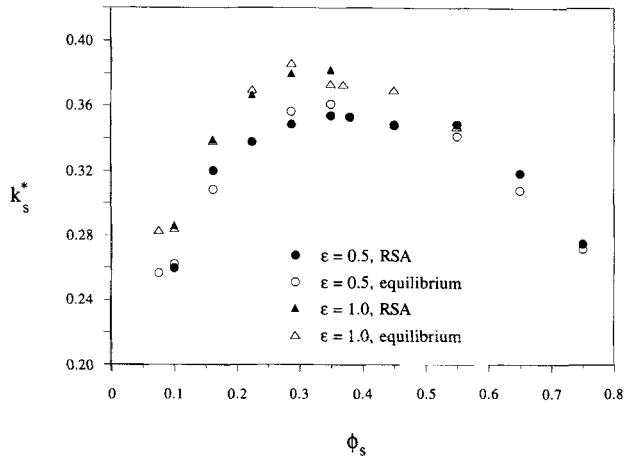

Figure 17. Dimensionless reaction rate, k_s^*, as a function of the volume fraction of inert support, ϕ_s, for different values of the impenetrability parameter, ϵ.

The parameters were set as follows: $R_a^* = 0.1$, $S^* = 0.05$. RSA and equilibrium systems were used to represent the inert support.

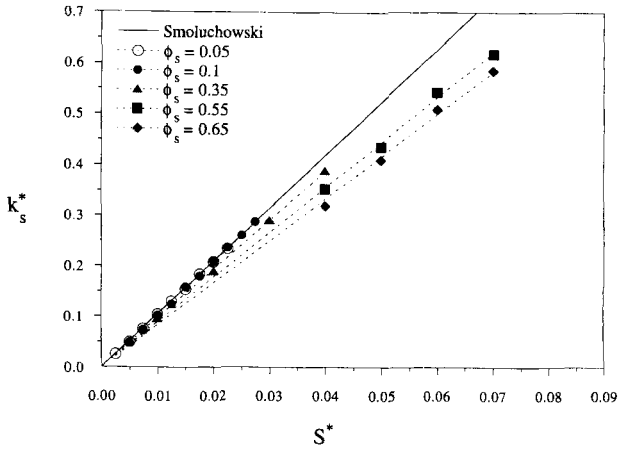

Figure 19. Dimensionless reaction rate, k_s^*, as a function of dimensionless specific surface area of active sites, S^*, for different values of the volume fraction of inert support, ϕ_s.

The parameters were set as follows: $R_a^* = 0.1$, $\epsilon = 0.5$. The dimensionless form of the result of Smoluchowski (1916), k_{Sm}^*, is represented by the solid line. Note that in these model catalysts, the active sites are unsupported. Curves through the origin have been fitted to guide the eye.

these plots, the standard errors are approximately 2%, the largest being 3%. Also plotted is the dimensionless form of the result of Smoluchowski (1916), k_{Sm} ($= 3D\phi_a/R_a^2$), which is valid for a system of unsupported active sites in the limit of a low density of sites:

$$k_{Sm}^* = \frac{k_{Sm}R_s^2}{D} = \frac{S^*}{R_a^*}. \tag{21}$$

At a low loading of active sites, the sites are far apart and the reaction rate must increase linearly with active site loading. It is of interest to compare the behavior of the supported catalyst in this "dilute" regime with the result of Smoluchowski (1916) for unsupported sites, as this gives a measure of the effect of the support at low catalyst loadings. The reason why the results for the model supported catalyst differ from the Smoluchowski result is as follows. With no inert support present, reactants are able to approach the active site from all directions. With the active site supported on an inert support, the range of angles from which the reactants are able to approach the active site is reduced. The effect of this "shielding effect," which increases with support volume fraction, is to reduce the reaction rate.

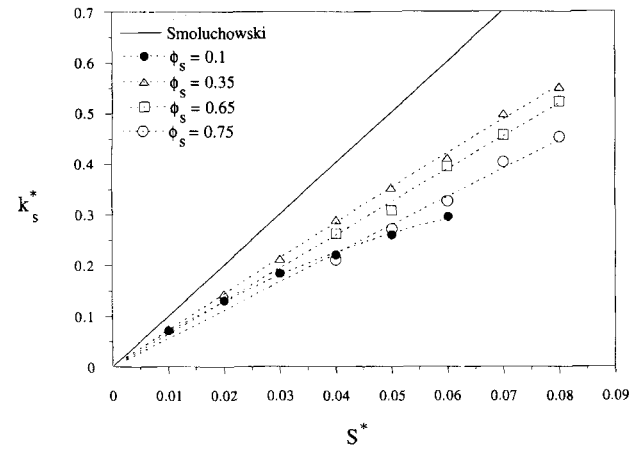

Figure 18. Dimensionless reaction rate, k_s^*, as a function of the dimensionless specific surface area of active sites, S^*, for different values of volume fraction of inert support, ϕ_s.

The parameters were set as follows: $R_a^* = 0.1$, $\epsilon = 0.5$. The dimensionless form of the result of Smoluchowski (1916), k_{Sm}^*, is represented by the solid line. Curves through the origin have been fitted to guide the eye.

Using the same values of ϵ and R_a^*, a further set of simulations were carried out in which the active sites were distributed randomly within the pore volume by RSA and not supported on the walls of the inert support (which is, of course, an unphysical situation). The plot in Figure 19 show k_s^* and the dimensionless result of Smoluchowski k_{Sm}^*, plotted as a function of S^*. The results for the low inert support volume fractions ($\phi_s \leq 0.35$) approach closely that predicted by the Smoluchowski result. Thus, for this model catalyst the primary effect of the support on the reaction rate at low catalyst loadings is via its effect on the local environment of the active site.

Summary and Discussion

Zheng and Chiew (1989) developed an FPT random walk method that they successfully applied to a system of static, unsupported active sites. This method has shortcomings when applied to supported catalysts. We have developed a new efficient FPT method and applied it to some simple supported catalysts, and the effect of the morphology of the catalyst on the reaction rate has been studied.

The effect of both the dispersion and loading of active sites

on the reaction rate was investigated. It was shown that for model-supported catalysts with a low active site loading, the reaction rate increases linearly with increasing loading of active sites, though at a lower rate than that predicted by the result of Smoluchowski (1916). Some simulations were carried out using model catalysts in which the active sites instead of being supported by the inert support were randomly distributed within the pore volume. These model catalysts, though unphysical, were used to show how for a low inert support volume fraction and low loading of unsupported active sites, the result of Smoluchowski accurately predicts the reaction rate. Thus, the primary effect of the support on the local reaction rate is by restricting access to the active site. Simulations carried out on model catalysts using a wide range of inert support fractions show that the inert support also affects the reaction rate through its effect on the dispersion of the active sites. The range of inert support volume fractions used in the simulations is wider than that found among commercial supported catalysts. Of course, the overall performance of the catalyst also depends on the transport of reactants from the surface of the particle to the active sites.

The simulations carried out on the model catalysts also show that the method by which the inert support is created (random sequential addition or equilibrium) has no effect on the results despite the fact that RSA and equilibrium structures are fundamentally different (Widom, 1966). This suggests that using RSA does not allow the generation of model solids with reaction properties that are significantly different from those of solids generated from equilibrium configurations.

The new method is specific to spherical particles. This is not a severe limitation since some commonly used catalyst supports, such as silica, alumina, and titania, consist of macroscopic aggregates of spherical particles. In addition, by varying the construction rules, models based on spherical elements have the capacity of representing a wider range of structures than we have investigated here. For example, it is possible following the creation of a configuration of spheres to simulate porosity changes due to sintering and compression (Reyes and Iglesia, 1991). Furthermore, the coordination number of PCS particles may be constrained to some maximum value, rather than being allowed to vary freely, which would allow more ramified structures to be generated.

In this work, the active material is deposited randomly within the pore space after the inert support has been prepared. However, the inert support in real catalysts is often impregnated with the active material prior to pelletizing. For the model catalyst used here, this would be equivalent to the addition of active sites to the spheres forming the inert support followed by the construction of the supported catalyst using these spheres. The distribution of the active material added this way would not be random but would be influenced by the packing arrangement of the spheres. Further, some of the active sites would be buried in the inert support, thus lowering the reaction rate. Our algorithm for the generation of the model catalyst can easily be adapted to reproduce this feature.

The emphasis of the work reported here was to develop the new simulation method, and to use it to investigate some aspects of the effect of the catalyst morphology on the reaction rate. Although no attempt was made to relate the parameters of the model to a particular real catalyst, we show in the Appendix that the parameter ranges used in this investigation are comparable to those of real amorphous catalysts. At present this simulation method is of value as a means of investigating the general reaction characteristics of supported catalysts. Before it can be used to make quantitative predictions for particular real catalysts, methods must be developed for the experimental determination of the structural parameters of the model. At present, standard experimental techniques for the physical characterization of porous solids, such as adsorption and mercury injection, are interpreted on the basis of lattice-based models. New analyses, in terms of continuum structural models, must be developed for these experiments. Finally, we note that work is in progress on the adaptation to more general kinetics.

Acknowledgment

This work was supported by the United Kingdom Science and Engineering Research Council and ICI Chemicals & Polymers Ltd.

Notation

c = length defined in Figure 3
P = the first passage time cumulative distribution function

Greek letters

τ = mean first passage time

Subscripts

p = connected with the sphere that forms the nondimpled surface
q = connected with the sphere that forms the surface of the dimple
s = inert support

Literature Cited

Arbabi, S., and M. Sahimi, "Computer Simulations of Catalyst Deactivation: I. Model Formulation and Validation," *Chem. Eng. Sci.*, **46**(7), 1739 (1991a).

Arbadi, S., and M. Sahimi, "Computer Simulations of Catalyst Deactivation: II. The Effect of Morphological, Transport, and Kinetic Parameters on the Performance of the Catalyst," *Chem. Eng. Sci.*, **46**(7), 1749 (1991b).

Beyne, A. O. E., and G. F. Froment, "A Percolation Approach for the Modelling of Deactivation of Zeolite Catalysts by Coke Formation," *Chem. Eng. Sci.*, **45**(8), 2089 (1990).

Bond, G. C., *Heterogeneous Catalysis Principles and Applications*, 2nd ed., Oxford Science Publications, Oxford (1990).

Hollewand, M. P., and L. F. Gladden, "Modelling of Diffusion and Reaction in Porous Catalysts Using a Random Three-Dimensional Network Model," *Chem. Eng. Sci.*, **47**(7), 1761 (1992).

Kim, I. C., and S. Torquato, "Determination of the Effective Conductivity of Heterogeneous Media by Brownian Motion Simulation," *J. Appl. Phys.*, **68**(8), 3892 (1990).

Kim, I. C., and S. Torquato, "Effective Conductivity of Suspensions of Hard Spheres by Brownian Motion Simulation," *J. Appl. Phys.*, **69**(4), 2280 (1991).

Kim, I. C., and S. Torquato, "Effective Conductivity of Suspensions of Overlapping Spheres," *J. Appl. Phys.*, **71**(6), 2727 (1992).

Lee, S. B., and S. Torquato, "Porosity for the Penetrable-Concentric-Shell Model of Two-Phase Disordered Media: Computer Simulation Results," *J. Chem. Phys.*, **89**(5), 3258 (1988).

McGreavy, C., J. S. Andrade, Jr., and K. Rajagopal, "Consistent Evaluation of Effective Diffusion and Reaction in Pore Networks," *Chem. Eng. Sci.*, **47**, 2751 (1992).

Melkote, R. R., and K. F. Jensen, "Computation of Transition and Molecular Diffusivities in Fibrous Media," *AIChE J.*, **38**, 56 (1992).

Metropolis, N., A. W. Rosenbluth, M. N. Rosenbluth, A. H. Teller, and E. Teller, "Equation of State Calculations by Fast Computing Machines," *J. Chem. Phys.*, **21**(6), 1087 (1953).

Miller, C. A., and S. Torquato, "Effective Conductivity of Hard Sphere Dispersions," *J. Appl. Phys.*, **68**(11) 5486 (1990).
Reyes, S. C., and E. Iglesia, "Effective Diffusivities in Catalyst Pellets: New Model Porous Structures and Transport Simulation Techniques," *J. Cat.*, **129**, 457 (1991).
Reyes, S. C., and E. Iglesia, in *Computer Aided Design of Catalysts and Reactors*, E. R. Becker, and C. J. Pereira, eds., Marcel Dekker, New York, 89 (1993).
Rikvold, P. A., and G. Stell, "D-Dimensional Interpenetrable-Sphere Models of Random Two-Phase Media: Microstructure and an Application to Chromatography," *J. Colloid Interf. Sci.*, **108**(1), 158 (1985).
Sahimi, M., "Transport of Macromolecules in Porous Media," *J. Chem. Phys.*, **96**, 4718 (1992).
Sahimi, M., G. R. Gavalas, and T. T. Tsotsis, "Statistical and Continuum Models of Fluid-Solid Reactions in Porous Media," *Chem. Eng. Sci.*, **45**(6), 1443 (1990).
Satterfield, C. N., *Heterogeneous Catalysis in Industrial Practice*, 2nd ed., McGraw-Hill, New York (1991).
Smoluchowski, M., *Phys. Z.*, **17**, 557 (1916).
Tassopoulos, M., and D. E. Rosner, "Simulation of Vapor Diffusion in Anisotropic Particulate Deposits," *Chem. Eng. Sci.*, **47**(2), 421 (1992).
Tomadakis, M. M., and S. V. Sotirchos, "Ordinary and Transition Regime Diffusion in Random Fiber Structures," *AIChE J.*, **39**(3), 397 (1993).
Torquato, S., "Bulk Properties of Two-Phase Disordered Media. 1. Cluster Expansion for the Effective Dielectric Constant of Dispersions of Penetrable Spheres," *J. Chem. Phys.*, **81**(11), 5079 (1984).
Torquato, S., and I. C. Kim, "Efficient Simulation Technique to Compute Effective Properties of Heterogeneous Media," *Appl. Phys. Lett.*, **55**(18), 1847 (1989).
Widom, B., "Random Sequential Addition to Hard Spheres to a Volume," *J. Chem. Phys.*, **44**(10), 3888 (1966).
Zhang, L., and N. A. Seaton, "Prediction of the Effective Diffusivity in Pore Networks Close to a Percolation Threshold," *AIChE J.*, **38**(11), 1816 (1992).
Zhdanov, V. P., "Application of Percolation Theory to Describing Kinetic Processes in Porous Solids," *Advances in Catalysis*, Vol. 39, Academic Press, New York (1993).
Zheng, L. H., and Y. C. Chiew, "Computer Simulation of Diffusion-Controlled Reactions in Dispersions of Spherical Sinks," *J. Chem. Phys.*, **90**(1), 322 (1989).
Zheng, L. H., and Y. C. Chiew, "Computer Simulation of Steady-State Diffusion Controlled Reaction Rates in Dispersion of Static Sinks: Effect of Sink Sizes," *J. Chem. Phys.*, **93**(4), 2658 (1990).

Appendix

In the following, we show how it is possible to create realistic model supported catalysts by assigning appropriate values to the parameters that constitute the set of construction rules. In real catalysts, the active material usually constitutes between 0.1 and 20% by weight of the total catalyst and is normally in the form of very small crystallites (1–50 nm in dia.) (Bond, 1990). In our example real catalyst, α-alumina and platinum are used as inert support and active material, respectively. The weight percentage of platinum is between 0.15 and 1.4 and the diameter of the platinum crystallites is 9 nm. The inert support volume fraction, ϕ_s, is set to 0.5 [typical approximate figure for commercial catalysts (Satterfield, 1991)] and the impenetrability parameter, ϵ, is set to 1 (alumina supports typically consist of macroscopic aggregates of spherical particles).

For a reactant undergoing bulk diffusion in the liquid phase, the order of magnitude of the mean free path will be the same as that of the molecular diameter of the reactant. To ensure that bulk diffusion takes place, the mean pore radius, r, within the supported catalyst must satisfy the following: $r \geq 30\lambda$ (Reyes and Iglesia, 1991). Using a reactant with a molecular diameter of 0.3 nm as an example, the mean pore radius ($= 100\lambda$) is 30 nm. [This is a typical dimension for a mesopore (Satterfield, 1991).] For the model-supported catalyst, the mean pore radius can be accurately predicted (Reyes and Iglesia, 1991) using the following equation based on nonintersecting uniform cylindrical pores:

$$r = 2V/A_s \tag{A1}$$

where A_s is the total surface area of the inert support.

The following calculations show that for this model supported catalyst, the appropriate values for the dimensionless specific surface area of active sites, S^*, corresponding to 0.15 and 1.4 wt. % of platinum are 0.008 and 0.08, respectively.

Physical data

Atomic weight of platinum = 195.09 mol^{-1}.
Molar volume of platinum metal (face-centered cubic packing) = 9.0909 $cm^3 \cdot mol^{-1}$.
Molecular weight of α-alumina (Al_2O_3) = 101.96 mol^{-1}.
Relative density of α-alumina = 3.97 cm^{-3}.
Molecular diameter of reactant = 0.3 nm.

Calculated quantities

For a system of nonoverlapping spheres, $V/A_s = R_s/3$.
Setting $r = 30$ nm, $R_s = 45$ nm (from Eq. A1).
R_a^* ($= R_a/R_s$) = 0.1.
Weight Al_2O_3 per cm^3 of supported catalyst = 1.985 g.
Weight percent per cm^3 of supported catalyst in the range (0.003–0.028) g.
Corresponding range of values for dimensionless specific surface area of active sites, S^*, = (0.008–0.08).

Manuscript received Dec. 28, 1993, and revision received Apr. 21, 1994.